π^+-p Interactions in the Energy Range around 500 Mev*

M. E. Blevins, M. M. Block, and J. Leitner
Duke University, Durham, North Carolina
(Received January 13, 1958)

A hydrogen-filled diffusion cloud chamber investigation of π^+-p interactions in the energy range around 500 Mev is reported. The elastic scattering angular distribution, based on a total of 180 events, is analyzed using only s and p waves, and also using s and p waves with a d-wave interference term. Phase shifts are presented and ambiguities are discussed. The d-wave contribution is small. The elastic cross section is used to compute the real part of the forward coherent scattering amplitude. The latter is in good agreement with that predicted by the dispersion relations. Inelastic production sets in at about 300 Mev. Eighteen inelastic events were found; 7 were $p+0$, 7 were n^{++}, and 4 were unidentifiable. Inelastic processes are discussed in terms of various models.

I. INTRODUCTION

POSITIVE pion-proton scattering experiments have been performed previously at energies up to 395 Mev.[1–3] There exists no conclusive evidence requiring the introduction of d waves in a phase shift analysis of the data, i.e., the data are, within experimental accuracy, satisfactorily described by s- and p-wave scattering. At higher energies one might expect significant contributions from d-wave scattering to be present, and it is of interest to see at what energies d waves become important.

Recently, dispersion relations for pion-proton scattering have been obtained by Goldberger *et al.*[4] There is good agreement between the existing π^+-p scattering data and the dispersion relations. However, Puppi and Stanghellini[5] have recently analyzed the π^--p low-energy data and found serious disagreement with theory. This disagreement might, among other things, indicate a breakdown of the principle of microscopic causality.[6] If so, it would be expected that the influence of this violation of causality would be more serious at the higher energies for positive-pion scattering.

In previous π^+-p scattering experiments up to 395 Mev,[3] there has been no evidence of inelastic scattering although the threshold for the production of an additional meson is only 170 Mev. The inelastic scattering angular distributions and charge state branching ratio are of interest in that they provide a means of comparing the many models of pion production.

The afore-mentioned features of π^+-p interactions have been studied in the energy range around 500 Mev using a hydrogen-filled cloud chamber in a magnetic field.

II. EXPERIMENTAL ARRANGEMENT

The experimental arrangement is shown in Fig. 1. A positive beam, produced by ramming a carbon target into the circulating 3-Bev proton beam of the Cosmotron, passed through a collimating channel in the loaded concrete Cosmotron shield. The beam momentum, 750±125 Mev/c, was selected by means of a steering magnet. The deflected beam, containing both pions and protons, passed through a graphite absorber and lead collimator, $8\frac{5}{8}$ in. wide by $2\frac{1}{2}$ in. high, into the chamber, which was situated in a concrete blockhouse. The chamber itself was a twenty-atmosphere, hydrogen-filled, diffusion cloud chamber[7] situated in a magnetic field of 10 000 gauss. The sensitive region was 16 in. in diameter and ~2 in. in depth.

The absorber in the path of the beam was 66 g/cm^2 thick and served to remove protons with momentum $\leqslant$840 Mev/c; those protons able to enter the chamber were so degraded in energy that they were heavily ionizing. It was calculated that the pions emerge with a mean momentum of 610±125 Mev/c. The measured momentum of 49 beam tracks was found to be 590

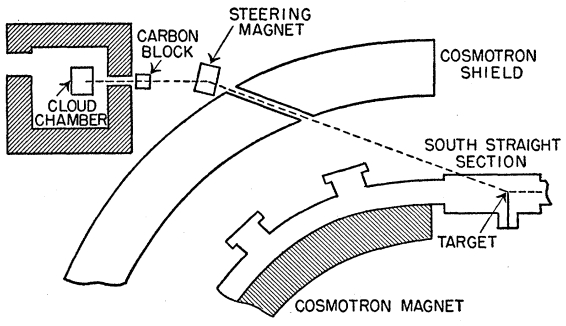

FIG. 1. Schematic of the experimental arrangement at the Cosmotron.

* This work was supported by the U. S. Atomic Energy Commission, and by the joint program of the Office of Naval Research and the U. S. Atomic Energy Commission.

[1] Anderson, Davidon, Glicksman, and Kruse, Phys. Rev. **100**, 279 (1955); J. Orear, Phys. Rev. **91**, 155 (1953); Anderson, Fermi, Martin, and Nagle, Phys. Rev. **96**, 1417 (1954); H. Anderson and M. Glicksman, Phys. Rev. **100**, 268 (1955).

[2] A. Mukhin *et al.*, in *Proceedings of the CERN Symposium on High-Energy Accelerators and Pion Physics, Geneva, 1956* (European Organization of Nuclear Research, Geneva, 1956), pp. 204–223.

[3] R. Margulies, private communication (to be published).

[4] Goldberger, Miyazawa, and Oehme, Phys. Rev. **99**, 986 (1955).

[5] G. Puppi and A. Stanghellini, Nuovo cimento **5**, 1305 (1957).

[6] Gell-Mann, Goldberger, and Thirring, Phys. Rev. **95**, 1612 (1954).

[7] Fowler, Fowler, Shutt, Thorndike, and Whittemore, Phys. Rev. **91**, 135 (1953).

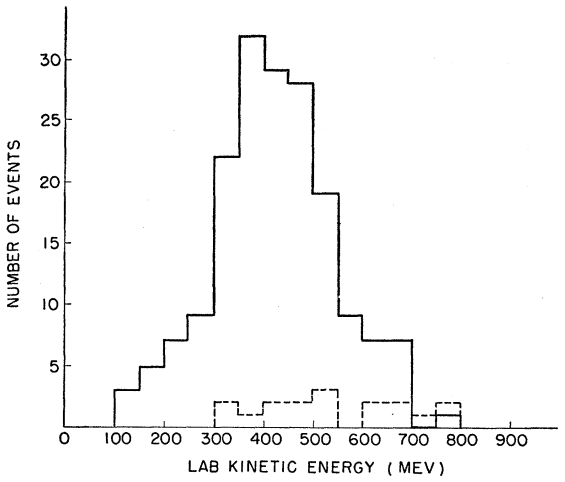

FIG. 2. The distribution of events as a function of the laboratory kinetic energy of the incoming pion. The solid histogram represents the elastic events and the dotted histogram represents the inelastic events.

± 80 Mev/c, in good agreement with the foregoing considerations.

III. SELECTION CRITERIA AND MEASUREMENT TECHNIQUE

An event was selected as a $\pi^+ - p$ interaction provided it satisfied the following criteria:

1. The incoming track was minimum ionizing.
2. The event vertex was unobscured.
3. The event did not occur within one inch of the chamber periphery (since bias against small-angle scattering events is high at the edges).
4. The incoming track was within the assigned beam angular dispersion limits. The angular dispersion of the beam was found by direct measurement at several points in the chamber. It was found that approximately 90% of the beam tracks lie within 4° of the mean beam direction at any point. Events with incoming pions lying outside this 90% region were discarded.

A reprojection apparatus,[8] in which each event was reconstructed in space on a screen which was free to rotate in three dimensions, duplicated as nearly as possible the optical system used to take the pictures. The direction of the incoming track was taken as the polar axis. The polar angles θ_π and θ_p of the scattered pion and proton, respectively, along with the azimuthal angles ϕ_π and ϕ_p were measured directly. Errors on the angles were assigned by repeating measurements several times for each event. A typical error in θ_p is $\pm 0.5°$.

The curvature of each track in an event was measured by plotting the track coordinates on a scale which exaggerates the sagitta. The plotted points were obtained by microscope measurement. The momentum of a track was taken as the linear average of that measured in each stereo view. The major source of error in momentum measurement was due to the short length of track available before the particle left the thin sensitive region.

Ionization estimates were made of all tracks in each event, using minimum beam tracks for comparison.

TABLE I. Correction factors for the number of events in the $0.9 \leqslant \cos\theta \leqslant 1.0$ interval.

Laboratory kinetic energy	ϕ correction	Coulomb correction	Total correction
335 Mev	1.56±0.20	0.89	1.39±0.20
420 Mev	1.31±0.14	0.87	1.14±0.14
525 Mev	1.29±0.20	0.89	1.15±0.20

[8] E. Fowler *et al.*, Rev. Sci. Instr. **25**, 996 (1954).

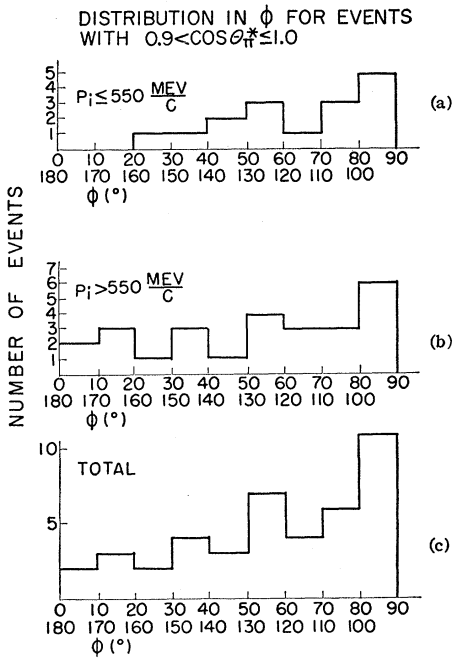

FIG. 3. Azimuthal angle (ϕ) distribution of events with center-of-mass scattering angle θ^*, such that $0.9 \leqslant \cos\theta^* \leqslant 1$. In diagram (c) the data are taken collectively, while in (a) and (b) the data with incoming pion momentum less than 500 Mev/c and greater than 500 Mev/c, respectively, are presented.

Each stereo pair was rough scanned twice, once by area scanning and once along the beam.

Approximately 39 000 pictures were taken with ~20 pions per picture. There were 178 elastic and 18 inelastic $\pi^+ - p$ interactions found within the fiducial region.

IV. ELASTIC EVENTS

A. Analysis

Elastic pion-proton scatterings are distinguished from other types of events on the basis of (1) coplanarity: an event was considered to be coplanar if ϕ_π was within ~2° of $\phi_p + 180°$; (2) satisfaction of the elastic

scattering kinematics, including ionization compatibility.

Five quantities were measured for each elastic event; the incoming pion momentum P_i, the two outgoing momenta P_π and P_p, the pion polar angle θ_π, and the proton recoil angle θ_p. These five quantities overdetermine the event, i.e., from any two of these the other three may be computed. The best fit quantities $\bar{P}_i$, $\bar{\theta}_p$ were obtained by minimizing R^2, where

$$R^2=\left(\frac{\bar{P}_i-P_i}{\sigma_{Pi}}\right)^2+\left(\frac{\bar{\theta}_p-\theta_p}{\sigma_{\theta p}}\right)^2+\left(\frac{P_\pi(\bar{P}_i,\bar{\theta}_p)-P_\pi}{\sigma_{p\pi}}\right)^2+\left(\frac{\theta_\pi(\bar{P}_i,\bar{\theta}_p)-\theta_\pi}{\sigma_{\theta\pi}}\right)^2+\left(\frac{P_p(\bar{P}_i,\bar{\theta}_p)-P_p}{\sigma_{Pp}}\right)^2,$$

via a graphical method,[9] as prescribed by the method of maximum likelihood. This procedure is the equivalent of making a weighted least-squares fit to the data.

There were 178 events identified as elastic π^+-p scatterings. The number of events as a function of incoming pion energy is shown in Fig. 2. Because of the large spread in incoming pion energy, the data were divided into two parts, 90 events with incoming π^+ energy between 275 Mev and 420 Mev and 88 events with incoming pion energy between 420 Mev and 850 Mev. Because of the asymmetric energy distribution, the mean energy of the low-energy group is 335 Mev and that of the high-energy group is 525 Mev. The energy distribution of the data taken collectively is reasonably symmetric and has a mean of 420 Mev.

TABLE II. Coefficients of (a) $d\sigma/d\Omega=\lambda^2(A+B\cos\theta+C\cos^2\theta)$ and (b) $d\sigma/d\Omega=\lambda^2(A+B\cos\theta+C\cos^2\theta+D\cos^3\theta)$.

		A	B	C	D
335 Mev[a]	(a)	0.196	1.55	2.75	
420 Mev	(a)	0.265±0.055	1.087±0.091	1.341±0.165	
	(b)	0.221	0.915	1.480	0.407
525 Mev	(a)	0.258±0.035	1.080±0.057	1.21±0.105	
	(b)	0.171	0.684	1.48	0.803

[a] See reference 14.

B. Corrections for Scanning Bias

The pion beam energy spectrum when multiplied by the total cross section[10] should give the energy distribution of the events. This has been compared to the observed event energy spectrum (Fig. 2). The expected and observed energy spectra are in good agreement, indicating that within the statistical accuracy, there is no energy-dependent scanning bias.

The distribution of the azimuthal angle ϕ for events with c.m. scattering angles $\theta \gtrsim 25°$ is isotropic, indicating no angle-dependent scanning bias for large-angle events. Figure 3 shows the ϕ distribution for $\theta<25°$; the anisotropy indicates a bias against small-angle events whose planes are perpendicular to the plane of the chamber. The requisite corrections for each grouping of the data are compiled in Table I.

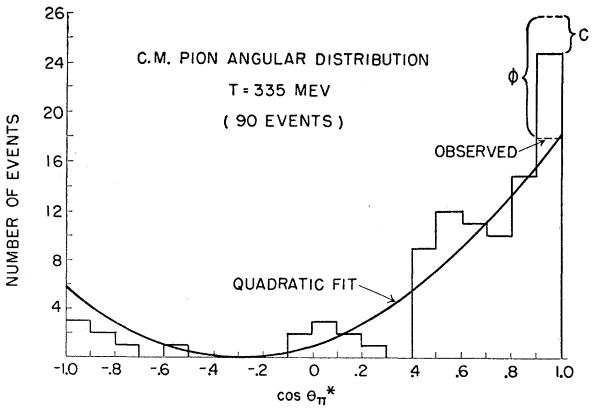

FIG. 4. The elastic scattering angular distribution in the c.m. system for events whose mean energy is 335 Mev. The Coulomb correction C and the azimuthal correction ϕ are indicated.

C. Angular Distribution and Phase Shift

The center-of-mass differential cross section is of the form $d\sigma/d\Omega=\lambda^2(A+B\cos\theta+C\cos^2\theta)$ if only s and p waves contribute to the scattering amplitude. A least-squares fit of the form $y=a+b\cos\theta+c\cos^2\theta$ was made to each of the observed angular distributions, by minimizing M^2, where[9]

$$M^2=\sum_{i=1}^{20}\left(\frac{y_i-y(a,b,c,\cos\theta_i)}{\sigma_i}\right)^2,$$

and σ_i is the standard deviation of y_i in the ith interval. Since we did not attempt to measure the total cross

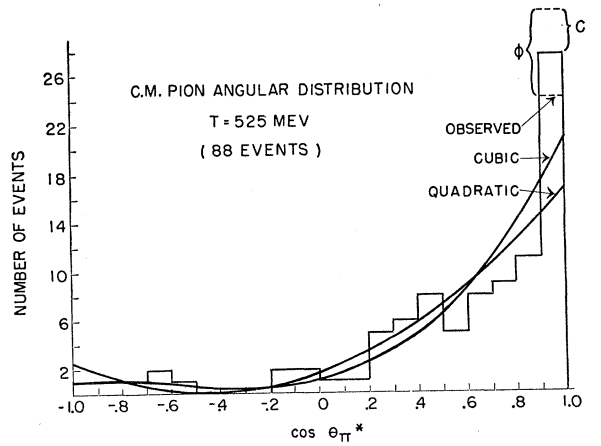

FIG. 5. The elastic scattering angular distribution in the c.m. system for events whose mean energy is 525 Mev. The Coulomb correction C and the azimuthal correction ϕ are indicated.

[9] For details see the thesis of M. Blevins, Duke University, 1957 (unpublished).

[10] S. Lindenbaum and L. Yuan, Phys. Rev. **100**, 306 (1955).

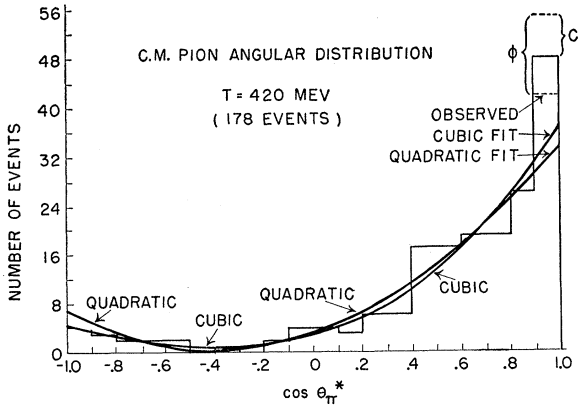

FIG. 6. The elastic scattering angular distribution in the c.m. system for the data taken collectively. The mean energy is 420 Mev. The Coulomb correction C and the azimuthal correction ϕ are indicated.

section, the fits were normalized to the total cross section as measured by counter methods.[10]

The shape coefficients A, B, and C so obtained were used to determine a preliminary set of phase shifts by the Ashkin method.[11] Using this preliminary set of phase shifts, the Coulomb interference term[12,13] was computed for each of the three groupings of the data and the correction factors are tabulated in Table I. The correction factor in the interval $0.9 \leqslant \cos\theta \leqslant 1.0$ is sufficiently small to justify the procedure of single iteration. The Coulomb correction is negligible for $\cos\theta < 0.9$.

After fully correcting the preliminary angular distributions, a second quadratic fit was made and the resulting final values of the shape coefficients are tabulated in Table II.[14] The final angular distributions are shown in Figs. 4, 5, and 6. These represent, respectively, the 90 events with a mean energy of 335 Mev, the 88 events with a mean energy of 525 Mev, and finally the data taken collectively with a mean energy of 420 Mev.

TABLE III. Phase shifts, in degrees.

	s, p phase shifts				
(Mev)	$\delta_3=\delta_3'$	δ_{31}	δ_{33}	δ_{31}'	δ_{33}'
335[a]	−28.0	−28.8	151.2		
420	−26.6±1.2	−32.5±1.1	161.1±0.3	−13.8±9.0	151.8±2.5
525	−28.1±5.1	−27.3±6.0	161.2±2.2	−15.5±10.6	155.3±2.5
	s, p, and d phase shifts				
	δ_3'	δ_{31}'	δ_{33}'	$\delta_3{}^d$	$\delta_5{}^d$
420	−27.5±5.3	−16.2±8.1	151.8	−6.3±6.5	+2.1±7.0
525	−29.2±7.1	−14.7±13.0	155.3	−9.3[b]	+2.1[b]

[a] See reference 14.
[b] The errors calculated for these phase shifts are so large (~20°) that the assumption of small d phase shifts is violated.

The values of A, B, and C in Table II were used to construct Ashkin plots from which the phase shifts were determined. The phase shifts and their errors[9] are tabulated in Table III. It should be emphasized that only the 335- and 525-Mev solutions are independent. The phase shifts for the data taken collectively are included since they can be determined with greater statistical accuracy.

The Ashkin plot for the collective angular distribution is shown in Fig. 7. It is clear that there can be no ambiguity in the value of δ_3, but δ_{31}, δ_{33}, and δ_{31}', δ_{33}' are equally valid solutions. One set of phase shifts, either the primed or the unprimed set, corresponds to the Yang solution, and the other set corresponds to the Fermi solution.[15] Because of large errors, it is not possible to determine unambiguously which solution is continuous with the phase shifts at lower energies. From the Ashkin plot it is clear that, if the Fermi solution is not very different from the Yang solution, $\delta_{31}-\delta_{33}$ is close to 180°. Since the contribution of spin-flip scattering to the differential cross section is proportional to $\sin(\delta_{31}-\delta_{33})$, the spin-flip scattering is very small in this energy region.

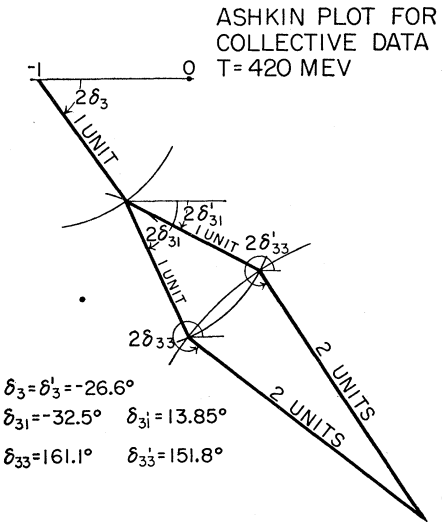

FIG. 7. The Ashkin graphical solution for the phase shifts representing the 420-Mev data.

If along with s and p waves, a d-wave interference term is considered, the differential cross section is of the form

$$d\sigma/d\Omega = \lambda\!\!\!^{-2}(A+B\cos\theta+C\cos^2\theta+D\cos^3\theta).$$

A fit of this form was made to the collective angular distribution (420 Mev) and to the 525-Mev group.

The quantity M was calculated for the quadratic

[11] J. Ashkin and S. Vosko, Phys. Rev. **91**, 1248 (1953).
[12] L. van Hove, Phys. Rev. **88**, 1358 (1953).
[13] F. Solmitz, Phys. Rev. **94**, 1799 (1954).
[14] The fitting method used gave a negative differential cross section for the 335-Mev data. By imposing the condition that $B^2-4AC=0$, a tangent fit is obtained. The shape coefficients A, B, and C of the tangent fit give a unique set of phase shifts $\delta_3=\delta_3'$, $\delta_{31}=\delta_{31}'$, and $\delta_{33}=\delta_{33}'$, i.e., there is no Fermi-Yang ambiguity.
[15] H. A. Bethe and F. de Hoffmann, *Mesons and Fields* (Interscience Publishers, Inc., New York, 1955), Vol. II, p. 72.

fits and the cubic fits and is tabulated in Table IV. Columns 2 and 3 show the expected average M values, $\bar{M}$, i.e., the number of experimental points less the number of free parameters, and the experimental value, M, calculated from Eq. (2) in the Appendix. In column 4 we have computed either

$$\int_M^\infty G(M)dM \Big/ \int_{\bar{M}}^\infty G(M)dM$$

or

$$\int_0^M G(M)dM \Big/ \int_0^{\bar{M}} G(M)dM,$$

for the cases $M \geqslant \bar{M}$, or $M \leqslant \bar{M}$, respectively, where $G(M)$ is the probability function given by Eq. (2) in the appendix. These integrals are the probabilities for a directional deviation as large as or greater than the experimentally observed deviation. This procedure is necessary to allow for the skewness of the probability curves $G(M)$ as shown in Fig. 12.

The expected value of M is 18 for the quadratic fits and 17 for the cubic fits (see the Appendix). The

TABLE IV. Expected average M values, $\bar{M}$, for quadratic and cubic fits, compared with experimental values. The reduced probabilities (see text) are also listed.

Lab. kinetic energy (Mev)	$\bar{M}$	M (exper)	Reduced probability
422 (quadratic fit)	18	14.1	48.9
(cubic fit)	17	11.7	31.8
520 (quadratic fit)	18	16.9	84.8
(cubic fit)	17	12.7	43.5

probabilities for the quadratic fits are somewhat greater than those of the cubic fits, suggesting that an s, p analysis is at least as meaningful as an analysis in terms of s, p phase shifts and d-wave interference terms.

Mukhin *et al.*[2] have obtained s, p, and d phase shifts for several energies up to 310 Mev and have stated that inclusion of d waves improves the fit to their angular distribution at 307 Mev. The basis of their conclusion is the apparently large discrepancy between their experimental M of 11.3 and the expected average value, $\bar{M}=5$ at this energy.

In Table V, we have tabulated their M values given for an s- and p-wave analysis alone, just as in Table IV. It is clear, from an examination of the relevant probabilities in column 4, that the fluctuation at 307 Mev is of the same order of severity as the fluctuation at either 310 Mev or 176 Mev. The fact that the experimental M exceeds $\bar{M}$ does not necessarily imply the inadequacy of the number of free parameters. This is as likely a statistical fluctuation as for M to be smaller than $\bar{M}$. It is certainly unreasonable not to expect statistical deviations as large as those observed by the Russian workers.

It may be seen from the Appendix that the M value

TABLE V. Expected average M values ($\bar{M}$), experimental M values, and reduced probabilities for s- and p-wave analysis alone.

Lab. kinetic energy (Mev)	$\bar{M}$	M (exper)	Reduced probability
176	6	1.7	9.6
200	4	5.7	51.0
240	4	4.4	82.1
270	3	5.0	40.9
307	5	11.3	10.4
310	5	1.2	6.2

is not a measure of the accuracy of an experiment. This is because the M value is the sum of the squares of the deviation from the theoretical curve in *units of the standard deviations* of the individual measurements, i.e., is scaled to the experimental accuracy. The accuracy of the experiment is, however, reflected in the errors computed for the calculated phase shifts shown in Table III. It is clear that the d-wave phase shifts are not well determined.

On the assumption that δ_{33} is relatively insensitive to the inclusion of d-wave interference terms in the differential cross section, the d phase shifts $\delta_3{}^d$ and $\delta_5{}^d$ have been found by the method described in reference 9. The d phase shifts are tabulated in Table III along with the compatible set of s and p phase shifts. The d phase shifts are seen to be quite small and do not seem to be required to fit the data within the limit of accuracy of this experiment.

Chew and Low[16] have proposed the equation $(\eta^3/\omega)\cot\delta_{33}=\frac{3}{4}f^2(1-\omega/\omega^*)$ for the energy dependence of δ_{33}. The notation is that of Chew.[17] A plot of $(\eta^3/\omega)\cot\delta_{33}$ *vs* ω with $f^2=0.08$ is shown in Fig. 8. For

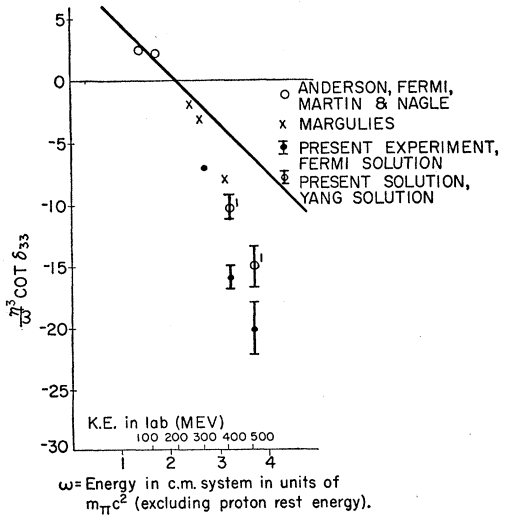

FIG. 8. The energy dependence of $(\eta^3/\omega)\cot\delta_{33}$. The solid line is the theoretical curve of Chew and Low.

[16] G. Chew and F. Low, Phys. Rev. **101**, 1570 (1956).
[17] G. Chew, in *Proceedings of the Fifth Annual Rochester Conference on High-Energy Physics* (Interscience Publishers, Inc., New York, 1955).

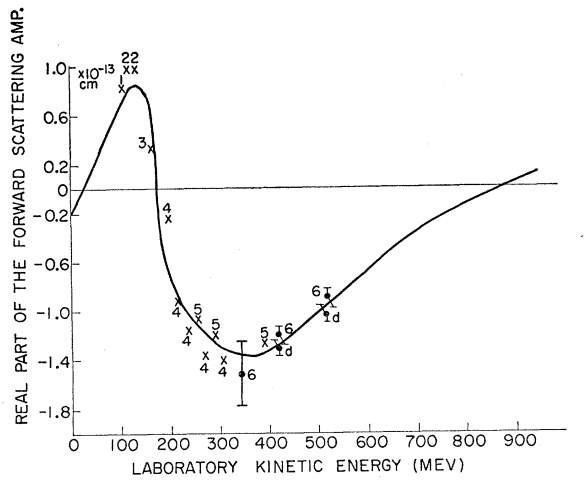

FIG. 9. The real part of the forward coherent scattering amplitude for π^+-p scattering *versus* laboratory kinetic energy. The solid curve is calculated from the dispersion relations. The numbers 1, 2, 3, 4, and 5 indicate, respectively, the data of J. Orear, Phys. Rev. **91**, 155 (1953); H. Anderson *et al.*, Phys. Rev. **96**, 1417 (1954); H. Anderson and M. Glicksman, Phys. Rev. **100**, 268 (1955); A. Mukhin *et al.*, in *Proceedings of the CERN Symposium on High-Energy Accelerators and Pion Physics Geneva, 1956* (European Organization of Nuclear Research, Geneva, 1956), pp. 204–223; and R. Margulies (private communication). The number 6 indicates data of present experiment based on *s*, *p* analysis, and *d* represents data based on *s*, *p*, *d* analysis.

comparison, the points obtained from previous experiments are plotted in Fig. 8 along with the values obtained in this experiment. Deviation from the theoretical curve starts at ~250 Mev and increases with increasing energy. This is not overly surprising, since at ~500 Mev there is appreciable inelastic scattering, indicating that two-meson processes contribute significantly, i.e., the one-meson approximation of Chew-Low is less applicable at higher energies.

Orear[18] has suggested the energy dependence of δ_3 and δ_{31} to be $\delta_3=-0.11\eta$, $\delta_{31}=0$. Within the accuracy of the experiment both the primed and unprimed solutions are in agreement with the above values, particularly upon the inclusion of *d* waves.

D. Comparison with the Dispersion Relations

Sternheimer[19] has computed the real part of the forward coherent scattering amplitude from the dispersion relations of Goldberger *et al.*,[4] using the total π^+-p and π^--p cross sections extrapolated to high energies. Figure 9 shows the π^+-p Sternheimer plot for laboratory energies up to 900 Mev.

The real part of the forward coherent scattering amplitude can be computed from measured quantities by means of the relation

$$\mathrm{Re}f_c(0^\circ)=\pm\{[d\sigma(0^\circ)/d\Omega]_{\mathrm{el}}-[d\sigma(0^\circ)/d\Omega]_{\mathrm{sf}}-[\mathrm{Im}f_c(0^\circ)]^2\}^{\frac{1}{2}}, \quad (1)$$

where $[d\sigma(0^\circ)/d\Omega]_{\mathrm{el}}$ = the elastic cross section at 0°, and $[d\sigma(0^\circ)/d\Omega]_{\mathrm{sf}}$ = the spin-flip cross section at 0°. The imaginary part of the forward coherent scattering amplitude can be obtained from the total cross section, σ_T, by means of the optical theorem, $\mathrm{Im}f_c(0)=\sigma_T/4\pi\lambda$.

The spin-flip amplitude, at all energies, must have a $Y_l^{\pm1}\propto\sin\theta$ angular dependence. It is therefore identically zero at $\theta=0°$. The elastic cross section at 0°, for each energy interval, is given directly by $\lambda^2(A+B+C)$, where the shape coefficients A, B, and C are tabulated in Table II. The experimental values of $\mathrm{Re}f_c(0°)$ obtained from (1), along with results from other experiments at lower energies,[1–3] are shown in Fig. 9. Comparison with the theoretical curve shows that agreement is well within the accuracy of the measurements at all energies. Note that the experimental error shown in Fig. 9 for the 335-Mev data is much larger than the statistical error. The tangent fit procedure[14] which places an additional constraint on the 335-Mev data is responsible for the large uncertainty. Experiment shows that at higher energies, $[d\sigma(0°)/d\Omega]_{\mathrm{el}}\gg\mathrm{Im}f_c(0°)$. Then $\mathrm{Re}f_c(0°)$ varies approximately as the square root of the forward elastic cross section and is thus not sensitive to small changes in the shape coefficients. Therefore the fit is equally good for either the *s*, *p* or the *s*, *p*, *d* analyses.

V. INELASTIC EVENTS

Inelastic events were identified by their failure to fit the elastic scattering kinematics. An event was classified by calculating the neutral mass, having determined the masses of the charged tracks from their momenta and ionizing power.

No inelastic event was found which could not be interpreted as single pion production; i.e., either $p+0$ or $n++$. Figure 2 shows the distribution of laboratory kinetic energy of the incoming pions for both elastic and inelastic events. Although the threshold for single pion production is 170 Mev, it is seen from Fig. 2 that the elastic to inelastic scattering ratio is zero up to 300 Mev. In the energy interval 300–575 Mev, the ratio is 0.06 ± 0.02 and increases to 0.42 ± 0.18 in the energy interval 576–750 Mev.

Of the total of 18 inelastic events found, seven were identified as $p+0$, seven as $n++$, one as either $p+0$ or $n++$; the remaining three were unmeasurable. Only 17 of these events are plotted in Fig. 2; the incoming momentum of the other event could not be determined.

Several models of inelastic pion scattering have been proposed: (1) the Fermi statistical model,[20] in which the reaction products achieve statistical equilibrium after collision and the final states are therefore distributed according to their statistical weights; (2) the isobar model,[21] in which a $(\frac{3}{2},\frac{3}{2})$ isobar is formed, which lives long enough to decay outside the range of nuclear

[18] J. Orear, Phys. Rev. **96**, 176 (1956).
[19] R. Sternheimer, Phys. Rev. **101**, 384 (1956).
[20] E. Fermi, Phys. Rev. **92**, 452 (1953).
[21] S. Lindenbaum and R. Sternheimer, Phys. Rev. **105**, 1874 (1957).

forces, thereby distributing the final states according to the probabilities for formation and decay of the isobar; (3) a model suggested by Kazes[22] in which the inelastic production is calculated using the static, single-meson formalism of Chew and Low.

Models (1), (2), and (3) predict charge state ratios $p+0/n++$ of $\frac{3}{2}$, 13/2, and $\frac{1}{2}$, respectively, to be compared with the experimental result of 7/7.

Figure 10 shows the center-of-mass momenta of the nucleons from both $p+0$ and $n++$ events plotted against $\cos\theta_N^*$, where θ_N^* is the nucleon scattering angle in the center-of-mass system. Figure 11 is a similar plot for pions from both $p+0$ and $n++$ events. The nucleons exhibit a preference for $\theta_N^*>90°$. This suggests that single pion production might be due to an interaction of the incident pion with the virtual pion surrounding the nucleon, and consequent stripping of this pion from the nucleon, with little momentum transfer to the nucleon.[23] For the sake of comparison, the phase-space momentum spectra of the statistical theory are also shown in Figs. 10 and 11.

VI. SUMMARY

Both s, p and s, p, d analyses have been carried out to obtain phase shifts for three energy intervals centered about 335, 420, and 525 Mev. The d-phase shifts, δ_3^d and δ_5^d, are small and do not seem to be required to fit the data. The Fermi and Yang solutions are extremely close and statistics are insufficient to distinguish between them by a continuity argument. The phase shifts δ_{31} and δ_3 are consistent with Orear's assignment of $\delta_{31}=0$ and $\delta_3=-0.11\eta$. The energy dependence of δ_{33} is in considerable disagreement with that predicted by Chew and Low. Since the Chew-Low plot includes recoil effects, the disagreement presumably indicates a breakdown of the one-meson approximation.

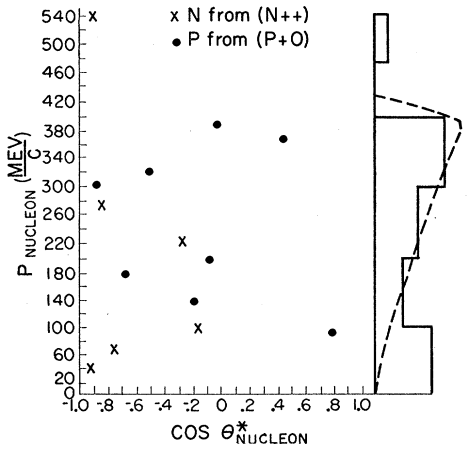

FIG. 10. The distribution of nucleon momenta *versus* scattering angle in the c.m. system. ● denotes protons from $p+0$ events. × denotes neutrons from $n++$ events. The dashed curve is the statistical-model momentum distribution.

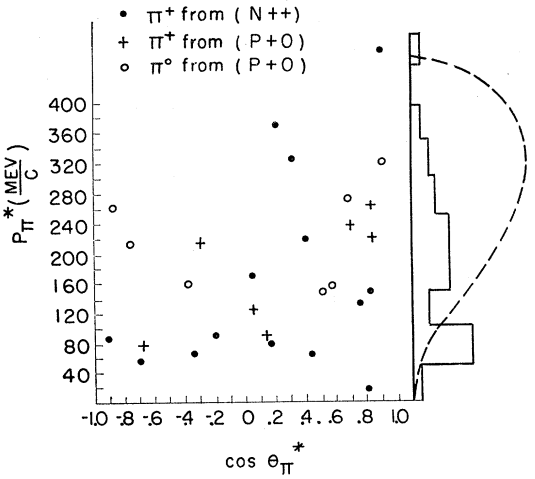

FIG. 11. The distribution of pion momenta *versus* center-of-mass scattering angle. o denotes π^0 from $p+0$ events. + denotes π^+ from $p+0$ events. ● denotes π^+ from $n++$ events. The dashed curve is the statistical-model momentum distribution.

The contribution of spin-flip scattering to the total cross section is small since $\delta_{31}-\delta_{33}\approx 180°$.

The real part of the forward coherent scattering amplitudes computed from the experimental forward elastic cross section is in good agreement with the $\mathrm{Re}f_c(0°)$ calculated by Sternheimer from the dispersion relations.

The ratio of inelastic to elastic scattering is effectively zero up to 300 Mev and rises to the order of 40% in the energy interval 575–750 Mev.

The $p+0/n++$ charge state ratio is found to be 7/7. The result is consistent with the ratios predicted by the statistical model and the model proposed by Kazes. It is not consistent with the isobar model. However, on the basis of the limited statistics involved, no strong conclusions on this point should be drawn. There is poor agreement between the experimental pion momentum distribution and the predicted spectrum of the statistical model.

The nucleon inelastic scattering angular distribution is peaked in the backward direction. This preference for small momentum transfer to the nucleon suggests that pion production might be due to a process of stripping of the pion from the physical nucleon.

ACKNOWLEDGMENTS

The authors would like to thank the Brookhaven National Laboratory Cloud Chamber Group of Dr. R. P. Shutt for their generosity in lending us the equipment which made this experiment possible. We also wish to express our thanks to Dr. E. M. Harth, Dr. I. S. Hughes, and Dr. G. G. Slaughter for many helpful discussions.

[22] E. Kazes, Phys. Rev. **107**, 1131 (1957).
[23] F. Dyson, Phys. Rev. **99**, 1037 (1955); A. Mitra, Phys. Rev. **99**, 957 (1955).

APPENDIX. DERIVATION OF THE PROBABILITY DISTRIBUTION OF THE M VALUE

If one is given that the curve $y(x)$ represents the value of a physical quantity y at x, e.g., y may be the differential cross section where x is the angle of scattering, then the M value for an experiment having n datum points is defined as

$$M=\sum_{i=1}^{n}\left(\frac{y(x_i)-y_i}{\sigma_i}\right)^2, \tag{2}$$

where x_i is the value of x at the midpoint of the ith experimental interval, y_i is the corresponding *experimentally measured* value of y at x_i, and σ_i is the standard deviation of the measurement assumed to have a Gaussian distribution and to be independent of the measured value. We define a Cartesian hyperspace of n dimensions where a coordinate y_i' of this space is defined as y_i/σ_i. Then

$$M=\sum_{i=1}^{n}[y'(x_i)-y_i']^2=r^2, \tag{3}$$

where r is the length of a vector in this hyperspace from the point $(y'(x_1), y'(x_2)\cdots y'(x_n))$ to $(y_1', y_2'\cdots y_n')$.

We note that the simultaneous probability of observing y_1 in dy_1, y_2 in dy_2, $\cdots y_n$ in dy_n for given values of $y'(x_1)y'(x_2)$, $\cdots y'(x_n)$ is given by

$$p(y'(x_1), \cdots y'(x_n), y_1'\cdots y_n')dy_1', dy_2'\cdots dy_n' = c_1\exp(-r^2/2)dy_1'dy_2'\cdots dy_n', \tag{4}$$

where c_1 is a normalization constant.

If we transform (4) to spherical hypercoordinates, and integrate out the angular variables, from (4) we can write $H(r)dr$, which is the probability that r lies in dr, as

$$H(r)dr=c_2r^{n-1}\exp(-r^2/2)dr, \tag{5}$$

where the factor r^{n-1} comes from the Jacobian of the volume element transformation, and c_2 is a new normalization constant.

Since from (3), $M=r^2$, (5) can be transformed so that $G(M)dM$, the probability that M lies in dM, is given by

$$G(M)dM=\frac{M^{(n-2)/2}}{2^{n/2}\Gamma(n/2)}e^{-M/2}dM, \tag{6}$$

where $\Gamma(n/2)$ is the gamma function of argument $n/2$.

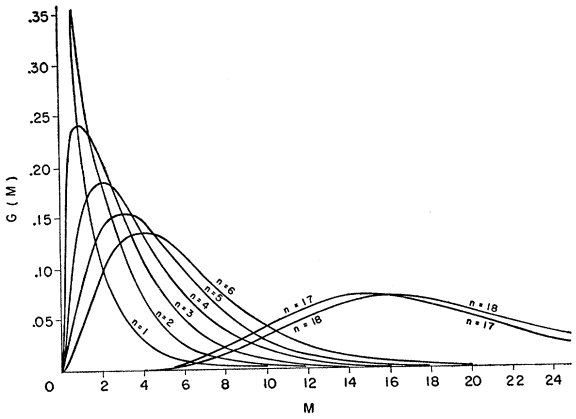

FIG. 12. The probability distribution $G(M)$ plotted as a function of the number of free parameters n.

From (6), we compute the average value of M to be $\bar{M}=n$, and also find that the variance is $\langle(M-\bar{M})^2\rangle_{Av}=2n$, and further that the most probable value of M is $n-2$. Figure 12 shows $G(M)$ plotted as a function of $n=1$, 2, 3, 4, 5, 6, 17, and 18.